

Quantum simulation of driven parabose oscillators

C. Huerta Alderete

Instituto Nacional de Astrofísica, Óptica y Electrónica, Calle Luis Enrique Erro No. 1, Sta. Ma. Tonantzintla, Pue. CP 72840, México

B. M. Rodríguez-Lara

Photonics and Mathematical Optics Group, Tecnológico de Monterrey, Monterrey 64849, Mexico.

Instituto Nacional de Astrofísica, Óptica y Electrónica, Calle Luis Enrique Erro No. 1, Sta. Ma. Tonantzintla, Pue. CP 72840, México.

E-mail: bmlara@itesm.mx

Abstract. Quantum mechanics allows paraparticles with mixed Bose-Fermi statistics that have not been experimentally confirmed. We propose a trapped-ion scheme whose effective dynamics are equivalent to a driven parabose oscillator of even order. Our mapping suggest highly entangled vibrational and internal ion states as the laboratory equivalent of quantum simulated parabosons. Furthermore, we show the generation of coherent oscillations and Gilmore-Perelomov parabose coherent states and their reconstruction from population inversion measurements in the laboratory frame. Our proposal, apart from demonstrating an analog quantum simulator of parabose oscillators, foreshadows the potential use of paraparticle dynamics in the design of quantum information systems.

1. Introduction

The harmonic oscillator is a fundamental building block of classical and quantum physics. In quantum mechanics, Wigner found that the equations of motion do not uniquely determine the Heisenberg-Born-Jordan relation for the quantum harmonic oscillator [1]. As a result, the community started exploring deformations of the harmonic oscillator. One such deformation was due to the reflection operator [2] and is known as the Calogero-Vasiliev oscillator [3,4]. In second quantization, the commutation relations for this model,

$$\begin{aligned} [\hat{A}, \hat{A}^\dagger] &= 1 + (p-1)\hat{\Pi}, \\ \{\hat{A}, \hat{A}^\dagger\} &= 2\hat{n} + p, \\ [\hat{n}, \hat{A}^\dagger] &= \hat{A}^\dagger, \quad [\hat{n}, \hat{A}] = -\hat{A}, \end{aligned} \tag{1}$$

deliver a paraboson algebra of order p [5]. Here, we have used the parity operator defined as $\hat{\Pi} = e^{i\pi\hat{n}}$, the operators \hat{n} , \hat{A}^\dagger , and \hat{A} are the number, creation and annihilation operators of the deformed oscillator, and the order parameter p is a positive integer, $p \in \mathbb{Z}^+$. Note that the standard boson algebra is recovered with order $p = 1$. Interestingly enough, quantum mechanics allows for the existence of paraparticles that have not been experimentally discovered as fundamental particles in nature [6,7].

On the other hand, trapped ions have proved a reliable platform for quantum simulation, offering high precision in both parameter control and measurement [8,9]. For example, quantum simulations of relativistic [10] and condensed matter [11] physics have been realized experimentally. In the following, we will provide an experimental proposal involving a single trapped ion driven by two pairs of orthogonal fields tuned to the first red- and blue-sideband transitions. Then, we will show that a particular parameter set-up allows for the simulation of an effective model equivalent to one of the orthogonal vibrational modes coupled to the two-level ion following Jaynes-Cummings and, the other, anti-Jaynes-Cummings dynamics. At this point, we will demonstrate that this effective model has at least one constant of motion that allows us to map it into a driven parabose oscillator of even order. We will discuss the different regimes and related measurements that are experimentally accessible and, as an explicit example, we will focus on the generation of coherent oscillations in the paraboson number and Gilmore-Perelomov parabose coherent states. We will also discuss how they can be reconstructed from population inversion measurements.

2. Experimental proposal.

Let us start with the experimental proposal. We consider a single trapped ion pumped by two pairs of orthogonal lasers in a configuration similar to the one we used to introduce

the cross-cavity quantum Rabi model [12],

$$\hat{H}_{ion} = \frac{1}{2}\omega_3\hat{\sigma}_3 + \sum_{j=1}^2 \left\{ \nu_j \hat{a}_j^\dagger \hat{a}_j + \sum_{k=-1,1} \Omega_{j,k} \times \right. \\ \left. \times \cos \left[\eta_{j,k} \left(\hat{a}_j^\dagger + \hat{a}_j \right) - \omega_{j,k}t + \phi_{j,k} \right] \hat{\sigma}_j \right\}. \quad (2)$$

The ion is described by the transition energy ω_3 and the Pauli matrices, σ_j with $j = 1, 2, 3$ fulfilling the $SU(2)$ commutation relation, $[\sigma_i, \sigma_j] = 2i\epsilon_{ijk}\sigma_k$. The two orthogonal vibrational modes of the ion center of mass motion are described by the mechanical oscillation frequencies ν_j and the creation (annihilation) operators, \hat{a}_j^\dagger (\hat{a}_j) with $j = 1, 2$ fulfilling the standard boson commutation relation, $[\hat{a}_j, \hat{a}_k^\dagger] = \delta_{j,k}$.

Working in the Lamb-Dicke regime, $\eta_{j,k}\sqrt{\langle \hat{a}_j^\dagger \hat{a}_j \rangle} \ll 1$, with one of each pair of driving fields tuned to the first blue- and the first red-sideband transitions plus a small detuning, $\omega_{j,k} = \omega_3 + k\nu_j + \delta_{j,k}$ with $k = \pm 1$, we set the pump fields small detunings to be equal, $\delta_{1,k} = \delta_{2,k} = \delta_k$, the phases to the values $\phi_{1,-1} = \phi_{1,1} = -\pi/2$, $\phi_{2,-1} = \pi$, and $\phi_{2,1} = 0$, and tune the driving field strengths to deliver just one effective coupling strength, $\Omega_{j,k}\eta_{j,k}e^{-\frac{1}{2}|\eta_{j,k}|^2} = g$. Then, we recover what we will call our laboratory frame Hamiltonian,

$$\hat{H}_{Lab} = \frac{1}{2}\omega_0\sigma_3 + \omega \left(\hat{a}_1^\dagger \hat{a}_1 + \hat{a}_2^\dagger \hat{a}_2 \right) + g \left[\left(\hat{a}_1^\dagger + \hat{a}_1 + \hat{a}_2^\dagger - \hat{a}_2 \right) \hat{\sigma}_+ + \text{h.c.} \right], \quad (3)$$

where the effective qubit frequency is given by the halved addition of small detunings $\omega_0 = -(\delta_{-1} + \delta_1)/2$ and the effective field frequencies by their halved difference, $\omega = (\delta_{-1} - \delta_1)/2$. This is a cross-cavity quantum Rabi model type Hamiltonian where the fields have equal frequencies and couple with the same strength to the qubit [12, 13]. It is well-known that it can be written as a Hamiltonian model where the ion is coupled under Jaynes-Cummings and anti-Jaynes-Cummings dynamics to each of the fields with identical effective coupling strength [12],

$$\hat{H}_{cc} = \frac{1}{2}\omega_0\hat{\sigma}_3 + \sum_{j=1}^2 \omega \hat{a}_j^\dagger \hat{a}_j + \sqrt{2}g \left[\left(\hat{a}_1^\dagger - \hat{a}_2 \right) \hat{\sigma}_+ + \left(\hat{a}_1 - \hat{a}_2^\dagger \right) \hat{\sigma}_- \right], \quad (4)$$

after using Schwinger two-boson representation of $SU(2)$ to effect a rotation $\hat{D}_y(\theta) = e^{i\theta\hat{J}_2}$ with $\theta = \pi/2$ and $\hat{J}_2 = -\frac{i}{2}(\hat{a}_1^\dagger \hat{a}_2 - \hat{a}_1 \hat{a}_2^\dagger)$. This new effective Hamiltonian conserves the scaled difference between population inversions from the two $SU(2)$ representations,

$$\hat{\eta}_{cc} = -2\hat{J}_3 + \frac{1}{2}(\hat{\sigma}_3 + 1), \quad (5)$$

where the effective population inversion in the two-boson representation of $SU(2)$ is given by $\hat{J}_3 = \frac{1}{2}(\hat{a}_1^\dagger \hat{a}_1 - \hat{a}_2^\dagger \hat{a}_2)$ and we have added the constant to make it always integer, $\hat{\eta}_{cc} = 0, \pm 1, \pm 2, \dots$. Note that this operator is composed by the excitation number from the Jaynes-Cummings and anti-Jaynes-Cummings models [14]. In the

laboratory frame, this operator,

$$\hat{\eta}_{\text{Lab}} = -2\hat{J}_1 + \frac{1}{2}(\hat{\sigma}_3 + 1), \quad (6)$$

is related to the population inversion of just the qubit and the mixing rate of the vibrational modes, $\hat{J}_1 = \frac{1}{2}(\hat{a}_1^\dagger \hat{a}_2 + \hat{a}_1 \hat{a}_2^\dagger)$, and, of course, it is a conserved variable, $[\hat{\eta}_x, \hat{H}_x] = 0$ with $x = \text{Lab}, cc$. At this point, we can make a stop and realize that the eigenstates of the vibrational state mixing rate are inherently entangled in the laboratory frame due to the \hat{D}_y rotation.

3. Diagonalization in the qubit basis

In order to isolate the field dynamics, we can move into a frame defined by the population inversion difference $\hat{\eta}_{cc}$ rotating at the qubit frequency ω_0 , implement a rotation of $\pi/4$ around $\hat{\sigma}_2$, and, then, diagonalize the resulting Hamiltonian in the qubit basis using the Fulton-Gouterman approach [15],

$$\begin{aligned} \hat{H}_{FG} &= \hat{U}_{FG} \hat{H} \hat{U}_{FG}^\dagger \\ &= \hat{H}_+ |e\rangle\langle e| + \hat{H}_- |g\rangle\langle g|, \end{aligned} \quad (7)$$

where the Fulton-Gouterman transform is the following,

$$\hat{U}_{FG} = \frac{1}{\sqrt{2}} \begin{pmatrix} 1 & \hat{\Pi}_{12} \\ 1 & -\hat{\Pi}_{12} \end{pmatrix}, \quad (8)$$

with the two fields parity defined as $\hat{\Pi}_{12} = e^{i\pi(\hat{a}_1^\dagger \hat{a}_1 + \hat{a}_2^\dagger \hat{a}_2)}$, such that the effective field Hamiltonians,

$$\begin{aligned} \hat{H}_\pm &= \sum_{j=1}^2 [\omega + (-1)^j \omega_0] \hat{a}_j^\dagger \hat{a}_j - \frac{(-1)^j}{\sqrt{2}} g \times \\ &\times \left\{ \hat{a}_j \left[1 \pm (-1)^j \hat{\Pi}_{12} \right] + \left[1 \pm (-1)^j \hat{\Pi}_{12} \right] \hat{a}_j^\dagger \right\}, \end{aligned} \quad (9)$$

describe two boson fields interacting through a nonlinear coupling that depends on the total parity. In summary, the mapping from the laboratory to the Fulton-Gouterman frame is provided by the unitary transformation,

$$\hat{T}_{\text{Lab} \rightarrow FG} = \hat{U}_{FG} e^{i\frac{\pi}{4}\hat{\sigma}_2} e^{i\omega_0 \hat{\eta}_{cc} t} e^{i\theta \hat{J}_2}. \quad (10)$$

The conserved operator in the Fulton-Gouterman frame becomes a different scaled difference of population inversions of the two $SU(2)$ representations,

$$\hat{\eta}_{FG} = \hat{\eta}_+ |e\rangle\langle e| + \hat{\eta}_- |g\rangle\langle g|. \quad (11)$$

where the operators associated to the excited and ground state diagonal components are diagonal themselves,

$$\hat{\eta}_\pm = -2\hat{J}_3 + \frac{1}{2} \left(1 \mp \hat{\Pi}_{12} \right) \quad (12)$$

such that, obviously, these pure field operators commute with their respective accompanying field Hamiltonian, $[\hat{H}_\pm, \hat{\eta}_\pm] = 0$. Thus, we can set ourselves to partition the whole Hilbert space into subspaces that keep the average of these operators constant.

4. Partition of the Hilbert space

Starting from the vacuum state and verifying the action of the effective field Hamiltonians, it is possible to partition the corresponding Hilbert spaces as

$$\mathcal{H}_{\pm} = \bigoplus_{N=0}^{\infty} \mathcal{H}_{\pm,N}, \quad (13)$$

where the subspaces are span by what we will identify later on as parabose Fock states of even order $p = 2(N + 1)$,

$$\begin{aligned} |+, 2N; k\rangle &= |-, 2N + 1; k\rangle = |h(k + 4N + 1), h(k)\rangle, \\ |+, 2N + 1; k\rangle &= |-, 2N; k\rangle = |h(k), h(k + 4N + 3)\rangle, \end{aligned} \quad (14)$$

with $N, k = 0, 1, 2, \dots$, and the following integer function,

$$h(k) = \frac{1}{4} (2k - 1 + e^{i\pi k}). \quad (15)$$

As expected, these subspaces conserve the difference in the population inversion,

$$\begin{aligned} \mathcal{H}_{+,2N}, \mathcal{H}_{-,2N+1} : \quad & \langle \hat{\eta}_{\pm} \rangle = -2N, \\ \mathcal{H}_{+,2N+1}, \mathcal{H}_{-,2N} : \quad & \langle \hat{\eta}_{\pm} \rangle = 2(N + 1), \end{aligned} \quad (16)$$

and cover it twice, once in the collection of subspaces $\mathcal{H}_{+,N}$ and once in the set of $\mathcal{H}_{-,N}$ subspaces. We can readily identify these subspaces in the laboratory frame as the eigenstates of Schwinger two-boson operator \hat{J}_1 for each and every representation defined by the total number of bosons in the vibrational modes.

5. Generalized Parabose oscillator

In these subspaces the effective field Hamiltonians are driven nonlinear oscillators,

$$\hat{H}_{\pm,N} = \omega (\hat{n}_N + N) \mp \frac{\omega_0}{2} e^{i\pi(\hat{n}_N+N)} \pm g (\hat{A}_N^{\dagger} + \hat{A}_N) + \lambda_{\pm,N}, \quad (17)$$

where the auxiliary constants are given in the following,

$$\begin{aligned} \lambda_{+,N} &= \omega_0 \left(N + \frac{1}{2} \right) e^{i\pi N}, \\ \lambda_{-,N} &= \left[\omega - \omega_0 \left(N + \frac{1}{2} \right) \right] e^{i\pi N} - \omega_0. \end{aligned} \quad (18)$$

and we have defined the creation and annihilation operators,

$$\begin{aligned} \hat{A}_N^{\dagger} &= \hat{a}_N^{\dagger} f_N(\hat{n}_N), \\ \hat{A}_N &= f_N(\hat{n}_N) \hat{a}_N, \end{aligned} \quad (19)$$

given in terms of a nonlinear deformation function,

$$f_N(k) = \sqrt{\frac{2k + (2N + 3) + (2N + 1) e^{i\pi k}}{2(k + 1)}} e^{i\pi(k+N)}, \quad (20)$$

and the standard boson operators for each subspace. We can calculate the actions of the nonlinear operators on the Fock states of each subspace,

$$\begin{aligned}\hat{A}_N^\dagger |\pm, N; k\rangle &= \sqrt{k+1} f_N(k) |\pm, N; k+1\rangle, \\ \hat{A}_N |\pm, N; k\rangle &= \sqrt{k} f_N(k-1) |\pm, N; k-1\rangle, \\ \hat{n}_N |\pm, N; k\rangle &= k |\pm, N; k\rangle,\end{aligned}\tag{21}$$

and, most important at this point, the action of this particular combination on the vacuum state of each subspace,

$$\hat{A}_N \hat{A}_N^\dagger |\pm, N; 0\rangle = 2(N+1) |\pm, N; 0\rangle,\tag{22}$$

suggest that each subspace corresponds to a paraparticle Hilbert space of even order $p = 2(N+1)$ [5]. Note that our quantum simulation will never provide ordinary bosons as they have odd order $p = 1$. It is straightforward to check that we have an even order parabose algebra in our hands,

$$\begin{aligned}[\hat{A}_N, \hat{A}_N^\dagger] &= 1 + (2N+1)\hat{\Pi}_N, \\ \{\hat{A}_N, \hat{A}_N^\dagger\} &= 2\hat{n}_N + 2(N+1), \\ [\hat{n}_N, \hat{A}_N^\dagger] &= \hat{A}_N^\dagger, \quad [\hat{n}_N, \hat{A}_N] = -\hat{A}_N,\end{aligned}\tag{23}$$

This helps us realize that the auxiliary field Hamiltonians,

$$\hat{H}_{\pm, N} = \frac{\omega}{2} \left\{ \hat{A}_N \pm \frac{g}{\omega}, \hat{A}_N^\dagger \pm \frac{g}{\omega} \right\} + F_{\pm, N}(\hat{n}_N),\tag{24}$$

are nothing else than displaced parabose oscillators plus an additional diagonal term that depends only on the parity,

$$F_{\pm, N}(\hat{n}_N) = \lambda_{\pm, N} - \omega \left(1 + \frac{g^2}{\omega^2} \right) \mp \frac{1}{2} \omega_0 e^{i\pi(\hat{n}_N + N)}.\tag{25}$$

6. Driven parabose oscillator dynamics

Note that in the case of $\omega_0 = 0$, that is small driving field detunings $\delta_{-1} = -\delta_1$, we recover a driven parabose oscillator of even order $p = 2(N+1)$,

$$\hat{H}_{Osc} = \omega \hat{n}_N + g \left(\hat{A}_N + \hat{A}_N^\dagger \right).\tag{26}$$

We will now study this model in order to provide a particular example and create some intuition. In the standard boson case, which is not covered by our quantum simulation, it is straightforward to identify two extremal cases, one for free evolution, $g = 0$, where an initial Fock state will only gather a phase proportional to the propagation time; in our simulation this regime does not make sense because it implies the absence of driving fields. And the other for pure driving, $\omega = 0$, where an initial Fock state will become a displaced number state due to the continuous pumping; this can be explored for parabosons with our quantum simulation. Another interesting regime for standard bosons occurs where the coupling is small with respect to the field frequency, $g \ll \omega$, here an initial Fock state will show coherent oscillations and also can be explored with

our quantum simulation. These behaviors for standard bosons are easily visualized in the so-called Glauber-Fock oscillator from photonic waveguide arrays [16,17]. In Fig. 1 we show that a similar type of dynamics occur in the driven parabose oscillator for the lowest order $p = 2$, that is $N = 0$. For example, let us consider as initial state, in the laboratory frame, the vacuum state of the subspace $\mathcal{H}_{+,0}$, that is, the ion in the ground state with vibrational modes cooled down to the lowest mechanical state,

$$|\psi(0)\rangle_{Osc} = |+, 0; 0\rangle \leftrightarrow |\psi(0)\rangle_{Lab} = |0, 0, g\rangle. \quad (27)$$

Note that this state is an eigenstate of pure Jaynes-Cummings dynamics. This initial state shows coherent oscillation of the mean paraboson number in the small coupling regime with $g = 0.1\omega$, Fig. 1(a). This coherent oscillation double the amplitude and have a slightly larger frequency than those obtained in the standard boson Glauber-Fock oscillator for exactly the same parameters. The mean paraboson number oscillation in the quantum simulation frame translate to oscillation of the population inversion in the laboratory frame, Fig. 1(b), because the latter is related to the parity of the parabose state,

$$\langle \hat{\sigma}_z \rangle_{Lab} = -\langle e^{i\pi \hat{n}_N} \rangle_{Osc}. \quad (28)$$

For pure driving, $\omega = 0$, the initial parabose vacuum state becomes a Gilmore-Perelomov parabose coherent state,

$$|\pm, N; \beta\rangle = e^{-ig(\hat{A}_N^\dagger + \hat{A}_N)t} |\pm, N; 0\rangle, \quad (29)$$

with coherent parameter equal to the scaled time, $\beta = -igt$, Fig. 1(c). In the laboratory frame we can write the $p = 2$ parabose coherent state as a non-separable state, for the sake of space we will write it one step before the laboratory frame,

$$\begin{aligned} |+, 0; \beta\rangle_{cc} = & \sum_{j=0}^{\infty} \frac{j!}{(2j)!} (\sqrt{2}gt)^{2j} {}_1F_1\left(j+1, j+\frac{1}{2}; -\frac{1}{2}g^2t^2\right) |j, j, g\rangle + \\ & -i \sum_{j=0}^{\infty} \frac{j!\sqrt{j+1}}{(2j+1)!} (\sqrt{2}gt)^{2j+1} {}_1F_1\left(j+2, j+\frac{3}{2}; -\frac{1}{2}g^2t^2\right) |j+1, j, e\rangle, \end{aligned} \quad (30)$$

where we have used the notation ${}_1F_1(a, b; z)$ for the confluent hypergeometric function. It is possible to confirm numerically that these states have balanced even and odd parity components for large coherent parameters. This can also be seen in the laboratory frame through the population inversion, Fig. 1(d).

In trapped ion experiments, the reconstruction of vibrational states from population inversion measurements is feasible. Thus, a viable measurement scenario would stop the evolution of the simulation, turn off the interactions, and recover phase space information from each of the vibrational modes at a time following standard methods [18–20]. This would allow to unmask the properties of parabose states, like the peculiar quadrature squeezing for a Gilmore-Perelomov parabose coherent state of order $p = 2$ shown in Fig. 2 using Husimi Q-function of the first vibrational mode in the laboratory

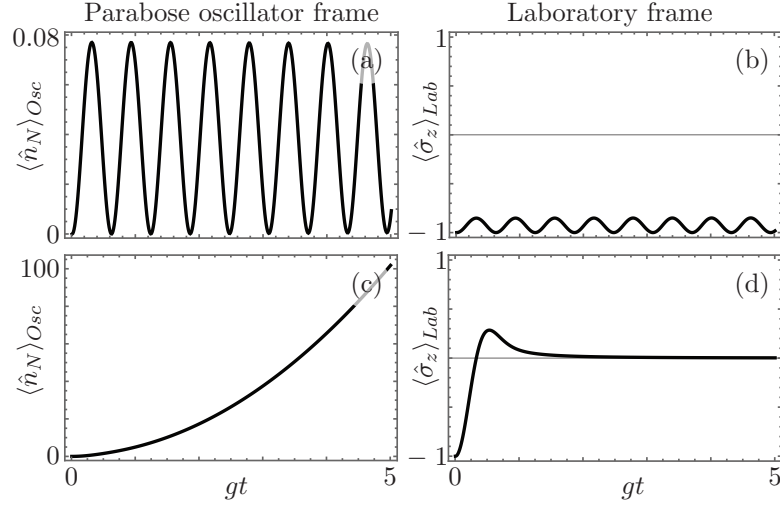


Figure 1. Time evolution of the mean parabose number operator, $\langle \hat{n}_N \rangle_{Osc}$, and corresponding population inversion in the laboratory frame, $\langle \hat{\sigma}_z \rangle_{Lab}$, for a starting $p = 2(N + 1) = 2$ parabose vacuum state under weak coupling, (a)-(b) $g = 0.1\omega$, and pure pumping, (c)-(d) $\omega = 0$, dynamics.

frame. We will cover the properties of Gilmore-Perelomov parabose coherent states in detail somewhere else.

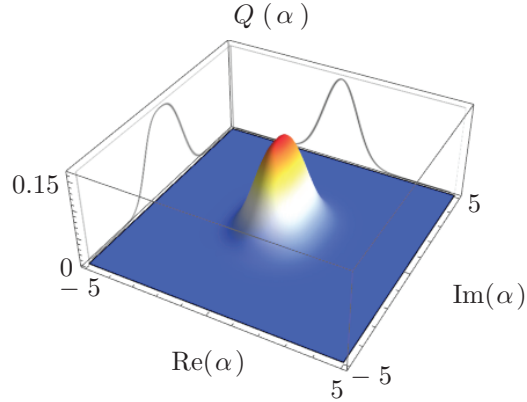


Figure 2. Husimi Q-function in the laboratory frame for the reduced density matrix of the first vibrational mode at scaled time $gt = 1$ under purely pumped dynamics, $\omega = 0$, and an initial state given by the parabose vacuum state of order $p = 2$.

7. Conclusion

In summary, we have proposed a trapped ion configuration where the interaction of the ion internal degree of freedom with two orthogonal center of mass motion degrees of freedom can be reduced to that of an even order parabose oscillator. We have discussed in detail both the experimental proposal and the analytic approach that diagonalizes the system for the internal degree of freedom and, then, partitions the Hilbert space for the

vibrational degrees of freedom delivering Hilbert subspaces corresponding to even order parabosons. As a particular example, we have focused on a pumped parabolose oscillator and demonstrated that it can produce coherent oscillations of the mean paraboson number and Gilmore-Perelomov parabolose coherent states that can be reconstructed in the laboratory frame through population inversion measurements.

Acknowledgments

C.H.A. acknowledges financial support from CONACYT doctoral grant #331166 and B.M.R.L. from CONACYT CB-2015-01 project #255230. The authors thank Changsuk Noh for fruitful discussions.

References

- [1] E. P. Wigner, “Do the equations of motion determine the quantum mechanical commutation relations?” *Phys. Rev.* **77**, 711 – 712 (1950).
- [2] L. M. Yang, “A note on the quantum rule of the harmonic oscillator,” *Phys. Rev.* **84**, 788 – 790 (1951).
- [3] F. Calogero, “Solution of a three-body problem in one dimension,” *J. Math. Phys.* **10**, 2191 – 2196 (1969).
- [4] M. A. Vasiliev, “Higher spin algebras and quantization on the sphere and hyperboloid,” *Int. J. Mod. Phys.* **6**, 1115 – 1135 (1991).
- [5] H. S. Green, “A generalized method of field quantization,” *Phys. Rev.* **90**, 270 – 273 (1953).
- [6] O. W. Greenberg and A. M. I. Messiah, “Selection rules for parafields and the absence of para particles in nature,” *Phys. Rev.* **138**, B1155 – B1167 (1965).
- [7] D. J. Baker, H. Halvorson, and N. Swanson, “The conventionality of parastatistics,” *Br. J. Philos. Sci.* **66**, 929 – 976 (2015).
- [8] M. Johanning, A. F. Varón, and C. Wunderlich, “Quantum simulations with cold trapped ions,” *J. Phys. B: At. Mol. Opt. Phys.* **42**, 154009 (2009).
- [9] R. Blatt and C. F. Roos, “Quantum simulations with trapped ions,” *Nature Phys.* **8**, 277 – 284 (2012).
- [10] C. F. Roos, R. Gerritsma, G. Kirchmair, F. Zähringer, E. Solano, and R. Blatt, “Quantum simulation of relativistic quantum physics with trapped ions,” *J. Phys. Conf. Ser.* **264**, 012020 (2011).
- [11] I. Arrazola, J. S. Pedernales, L. Lamata, and E. Solano, “Digital-analog quantum simulation of spin models in trapped ions,” *Sci. Rep.* **6**, 30534 (2016).
- [12] C. H. Alderete and B. M. Rodríguez-Lara, “Cross-cavity quantum Rabi model,” *J. Phys. A: Math. Theor.* **49**, 414001 (2016).
- [13] S. A. Chilingaryan and B. M. Rodríguez-Lara, “Exceptional solutions in two-mode quantum Rabi models,” *J. Phys. B: At. Mol. Opt. Phys.* **48**, 245501 (2015).
- [14] B. M. Rodríguez-Lara, H. Moya-Cessa, and A. B. Klimov, “Combining Jaynes-Cummings and anti-Jaynes-Cummings dynamics in a trapped-ion system driven by a laser,” *Phys. Rev. A* **71**, 023811 (2005).
- [15] A. Moroz, “Generalized Rabi models: diagonalization in the spin subspace and differential operators of Dunkl type,” *Europhys. Lett.* **113**, 50004 (2016).
- [16] B. M. Rodríguez-Lara, “Exact dynamics of finite Glauber-Fock photonic lattices,” *Phys. Rev. A* **84**, 053845 (2011).
- [17] L. V. Vergara and B. M. Rodríguez-Lara, “Gilmore-Perelomov symmetry based approach to photonic lattices,” *Opt. Express* **23**, 22836–22846 (2015).

- [18] J. F. Poyatos, R. Walser, J. I. Cirac, P. Zoller, and R. Blatt, “Motion tomography of a single trapped ion,” *Phys. Rev. A* **53**, 1966 – 1969 (1996).
- [19] C. D’Helon and G. J. Milburn, “Reconstructing the vibrational state of a trapped ion,” *Phys. Rev. A* **54**, 25 – 28 (1996).
- [20] D. Leibfried, D. M. Meekhof, B. E. King, C. Monroe, W. M. Itano, and D. J. Wineland, “Experimental determination of the motional quantum state of a trapped atom,” *Phys. Rev. Lett.* **77**, 01713 – 01719 (1996).